RADAR ALTIMETRY

Diverse Applications The primary objective of radar altimetry from satellites is to measure the topography of the ocean surface (Figure 1). In the next two classes we'll cover applications of radar altimetry. The technical discussion, presented here, is motivated by the precision and accuracy requirements of the most common applications as shown in Table 1.

Table 1. Scientific applications of radar altimetry

Feature	**Amplitude**	**Horizontal Scale**	**Timescale**
geoid	30 m	10,000 km	∞
dynamic topography	1 m	10,000 km	∞
climate changes	0.01 m	10,000 km	10 - 100,000 yr
tides	0.2-2 m	100 - 10,000 km	lunar and solar freq.
El Nino	0.1 m	6,000 km	~5 yr
fronts and eddies	0.3 m	100 - 1000 km	~1 mo
seamounts	1 m	50 km	∞
ridge axes	0.02 m	10 km	∞

These applications span a wide range of measurement requirements. The most stringent applications are *climate change* and small-scale gravity features such as *ridge axes*. The gravity applications require a point-to-point precision of 0.02 m which is very difficult to achieve when 1 m tall ocean waves are present. The climate change application requires a 0.01 m accurate altimeter over a much longer horizontal scale. In addition to a problem with electromagnetic bias due to ocean waves, this application also requires a 0.01 m knowledge of the absolute spacecraft position over a 10 year plus timescale. All of the applications requiring high accuracy at long wavelength also require an accurate knowledge of the delay of the radar echo as it passes through the ionosphere, the dry part of the atmosphere, and the wet (variable) part of the troposphere. It is also apparent that one person's signal is another person's noise so, for example, most applications require removal of the tidal signal to correct the data although there are scientists who use altimeter data to observe the tidal signal. First I discuss the engineering and environmental factors

effecting the precision of the altitude measurement *H*. Then I'll discuss the tide and path corrections.

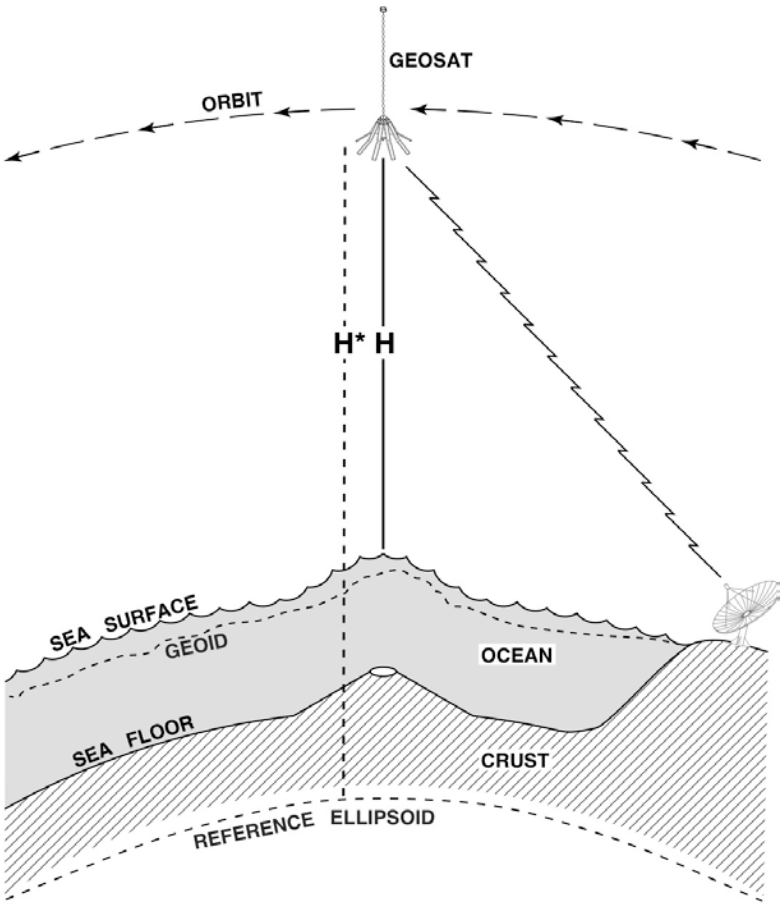

Figure 1. Schematic diagram of the GEOSAT altimeter measuring its altitude *H* above the closest point on the ocean surface using a pulse-limited radar. Satellite tracking is used to determine the height of the satellite above the reference ellipsoid *H**. The difference between *H** and *H* is the height of the ocean surface which consists of a time invariant geoid height plus the tide height plus ocean dynamic topography.

Beam-Limited Footprint As discussed earlier in the course, the radar altimeter operates in the microwave part of the spectrum so the method has the following attributes: the atmosphere is very transparent at 13 GHz; there is little stray radiation coming from the Earth; and the illumination pattern on the surface of the ocean is very broad for reasonable sized antennas. As derived previously, the angular resolution θ_r of a circular aperture having radius D is given by $\sin\theta_r = 1.22\lambda / D$ where λ is the wavelength of the radar (Figure 2). Suppose we have a 1 m diameter radar operating at a wavelength of 22 mm (Ku-band) and this is mounted on a satellite orbiting at an altitude of 800 km. The diameter of the illumination pattern on the ocean surface is given by

$$D_s = 2H\sin\theta_r \cong 2.44\,H\frac{\lambda}{D} \qquad (1)$$

where we have assumed $\tan\theta_r \cong \sin\theta_r$. The illumination diameter or *beam width* of the radar is quite large (43 km). Using this configuration, it will be impossible to achieve the 10 km horizontal resolution required for the gravity anomaly applications. However, one benefit of this wide illumination pattern is that small (~1 degree) pointing errors away from *nadir* are not a problem.

To achieve the 0.02 m range resolution needed for several of the above applications, one must measure the travel time of the radar echo to an accuracy of

$$\Delta t = \frac{2\Delta h}{c} = 1.3x10^{-10}s. \qquad (2)$$

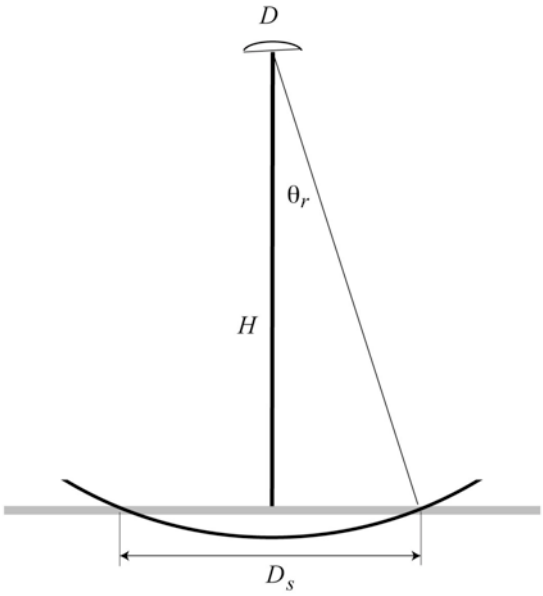

Figure 2 Schematic diagram showing the beam-limited footprint of a radar altimeter.

This can be translated into the bandwidth of the signal needed to form such a sharp pulse $\Delta\nu = 1/\Delta t$. In this case a 8 GHz bandwidth is needed. Note that the carrier frequency of the radar altimeter is only 13 GHz so the pulse must span most of the electromagnetic spectrum. Can

you imagine all of the electronics that would be effected when this radar passed over a major city such as Los Angeles. Obviously we can't use the entire EM spectrum so we'll have to live with a bandwidth of only 0.3 GHz. However, it turns out that ocean waves effectively limit the accuracy of the travel time measurement so a 0.3 GHz bandwidth is adequate. We'll just have to do a lot of averaging to reduce the noise.

Pulse-limited Footprint Assume for the moment that the ocean surface is perfectly flat (actually ellipsoidal) but has point scatters to reflect the energy back to the antenna. The radar forms a sharp pulse having a duration t_p of about 3 nanoseconds corresponding to the 0.3 GHz bandwidth. In practice, to reduce the peak output requirement of the transmitter, the radar emits a frequency-modulated chirp having a much lower amplitude but extending over a longer period of time. The chirped radar signal reflects from the ocean surface and returns to the antenna where it is convolved with a *matched filter* to regenerate the desired pulse. This is a common signal processing technique used in all radar systems. After the matched filter one can treat the measurement as a pulse. We'll initially assume a square wave pulse of length $l_p = ct_p / 2$ but later we'll use a Gaussian shape which is a better approximation to the actual pulse shape. The diagram below illustrates how the pulse interacts with a flat sea surface. When the leading edge of the spherical wavefront first hits the ocean surface the footprint is a point. More energy arrives until the trailing edge of the waveform arrives. We define the *pulse-limited footprint* r_p as the radius of the leading edge of the pulse when the trailing edge of the pulse first hits the ocean surface.

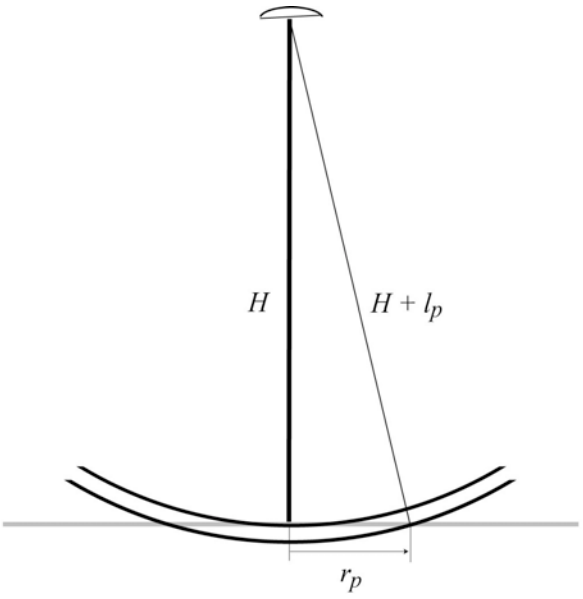

Figure 3. Schematic diagram showing the configuration when the trailing edge of the pulse arrives at the flat ocean surface.

The radius of the outer edge of the illumination pattern is found by using Pythagoreans theorem as shown in Figure 3

$$H^2 + r_p^2 = \left(H + l_p\right)^2 = H^2 + l_p^2 + 2Hl_p \tag{3}$$

where r_p is the radius of the leading edge of the pulse. The H^2's cancel and we can assume l_p^2 is very small compared with the other terms so the pulse radius is

$$r_p = \left(2Hl_p\right)^{1/2} = \left(Hct_p\right)^{1/2}. \tag{4}$$

For a 3 ns pulse length, the pulse radius is 0.85 km so the diameter or *footprint* of the radar is 1.7 km. This footprint is much less than the beam width so the pulse-limited approach is adequate for recovering the gravity field at 10 km length scales.

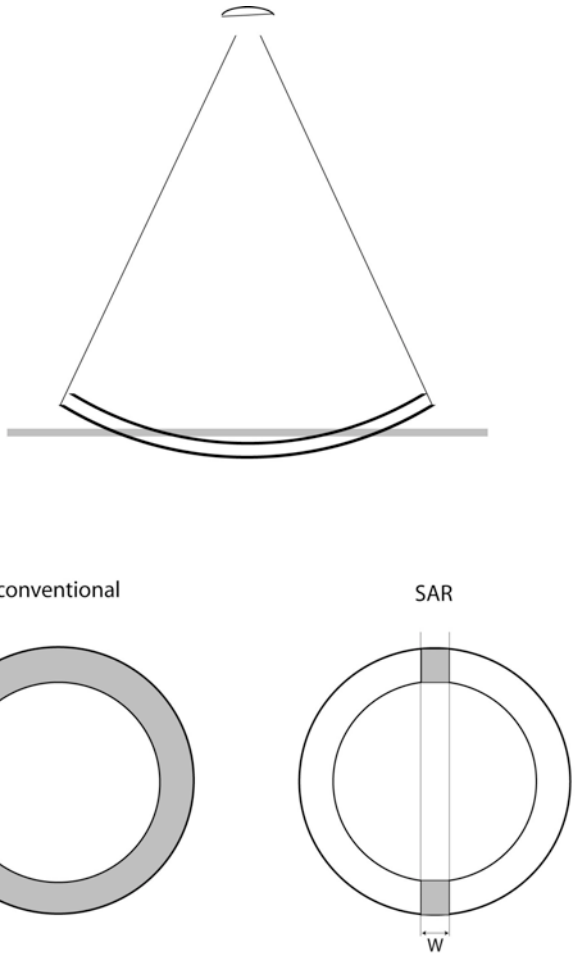

Figure 4. Schematic diagram of the pulse at a time after the trailing edge arrival time. The radaii of both the leading edge and trailing edge increase with time. For the conventional radar, the interaction area remains constant with time while for the SAR (discussed below), the interaction area decreases as the square root of time.

The power versus time for the pulse of length t_p that has been reflected from a perfectly flat ocean is easily calculated using the time evolution of the footprint shown in Figure 4 (left). We assume that power is linearly related to the area of the ocean illuminated. This power versus time function has three parts - the time before the leading edge of the pulse arrives, the time between the leading and trailing edge arrival time, and the time after the trailing edge arrives. The area versus time equation is

$$P(t) = \left\{ \begin{array}{cc} 0 & t < t_o \\ \pi r^2(t) & t_o < t < t_o + t_p \\ \pi\left[r^2(t) - r^2\left(t - t_p\right)\right] & t > t_o + t_p \end{array} \right\}. \qquad (5)$$

Using the pulse radius versus time given in equation (4), and normalizing by the peak power, the power versus time function is

$$P(t) = \left\{ \begin{array}{cc} 0 & t < t_o \\ \dfrac{(t - t_o)}{t_p} & t_o < t < t_o + t_p \\ 1 & t > t_o + t_p \end{array} \right\} \tag{6}$$

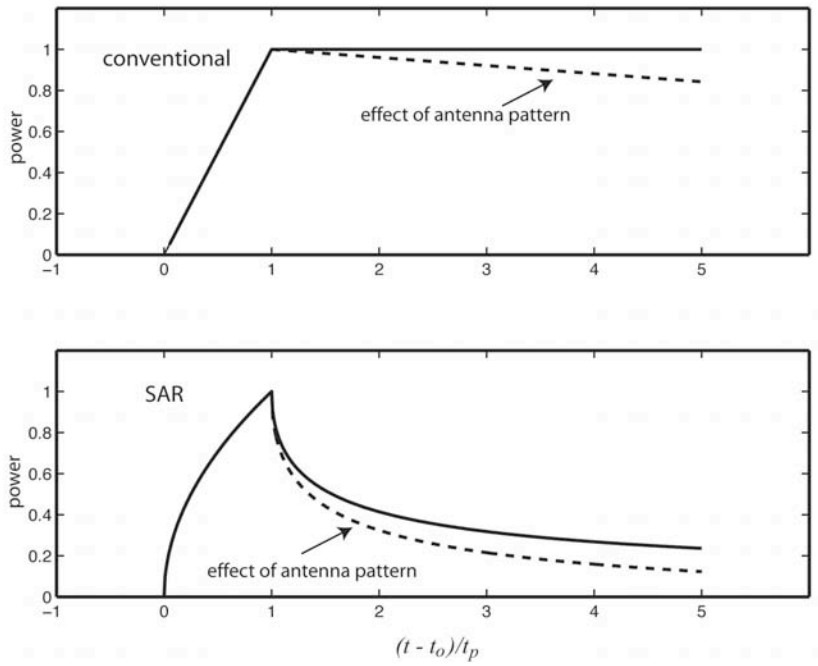

Figure 5. Schematic diagram of power versus time for a conventional pulse-limited radar altimeter (upper) and a SAR altimeter (lower). The leading edge arrival time is zero and the normalized pulse duration is 1.

A diagram of the power versus time is shown in Figure 5 (top). The power begins to ramp-up at time zero and the ramp extends for the duration of the pulse. At times greater than the pulse duration the diameter of the radar pulse continues to grow and energy continues to return to the radar. The power should be constant with time according to equation 6 because the area remains constant with time. However, the power of the reflected pulse actually decreases gradually with time according to the illumination pattern of the radar on the ocean surface.

SAR Altimeter The technique of synthetic aperture radar (SAR) can be used to sharpen the footprint of the pulse in the along-track direction. We discuss this more thoroughly later in the course when we introduce the concepts of synthetic aperture radar. For now, consider the CryoSat radar altimeter that sends out pulses at a rate of 18,000 per second. The ground speed of the satellite is about 6800 m/s so the radar moves 0.38 m between pulses which is less than 1/2 the diameter of the radar antenna. This high sampling rate ensures that the pulses can be summed coherently to form a longer synthetic aperture [*Raney*, 1998]. The two-way travel time of a single pulse is 5.3 ms. To avoid sending new pulses while recording old pulses, the pulses are sent in bursts of duration less than the two way travel time. In this case the maximum number of pulses that could be sent without overlap of transmit and receive is 96. In practice it is common to send 64 pulses in a burst since this is a power of 2 which also facilitates Fourier transform processing. One should record for at least as long as the duration of a burst. In the case of CryoSat the inter burst interval is about 2 times longer than needed or 11.7 ms. Coherent summation of echos over the burst interval is used to form a synthetic aperture L of length 48 m. Using Fraunhoffer diffraction theory, the length of the pulse on the ocean surface from zero crossing to zero crossing is approximately 653 m. The -3dB beamwidth of the power illumination pattern is 272 m. This sharpened pulse of length W is shown as the shaded area in Figure 3 (lower right).

To determine the power versus time function for a SAR waveform, we'll make an approximation that W is much less than the pulse-limited footprint described above of 1700 m [*Raney*, 1998]. In this case we still have three segments to the power versus time function - the time before the leading edge of the pulse arrives, the time between the leading and trailing edge arrival time, and the time after the trailing edge arrives. We approximate the illumination pattern for the second segment as a single rectangle of width W and length of twice the leading edge radius. We approximate the third segment as two rectangles of width W and length equal to the difference between the leading edge pulse radius and the trailing edge pulse radius as shown in Figure 4 (lower right). Under these simplifying assumptions, the power versus time function is

$$P(t)=\begin{Bmatrix} 0 & t<t_o \\ 2Wr(t) & t_o<t<t_o+t_p \\ 2W\left[r(t)-r\left(t-t_p\right)\right] & t>t_o+t_p \end{Bmatrix} . \quad (7)$$

As derived above, the radius versus time function is given by $r=(Hct)^{1/2}$. Inserting this into equation 7 one finds the following form for the normalized power versus time function where time is now relative to the arrival time of the leading edge $t'=t-t_o$.

$$P(t')=\begin{Bmatrix} 0 & t'<0 \\ \left(\frac{t'}{t_p}\right)^{1/2} & 0<t'<t_p \\ \left(\frac{t'}{t_p}\right)^{1/2}-\left(\frac{\left(t'-t_p\right)}{t_p}\right)^{1/2} & t'>t_p \end{Bmatrix} \quad (8)$$

The pulse shape of the SAR-altimeter is very different from the pulse shape of the pulse-limited altimeter as shown in Figure 5 (lower). On the leading edge the power increases as the square root of time. The main difference is the trailing edge where the SAR-mode pulse decreases as the square root of time while the pulse-limited altimeter has a uniform power with time until the pulse radius approaches the beam-limited footprint of the radar.

For ocean altimetry there are two main benefits to this SAR altimetry approach. First because all 64 waveforms within a burst are being summed coherently into a single aperture, the overall summed signal of the SAR-altimeter is 64 times greater than the conventional pulse-limited altimeter. This enables one to build a radar that uses less power per pulse [*Raney*, 1998]. Note the pulse repetition frequency is higher by a factor of 9 but the duration of the burst is only 1/3 the length of the inter burst interval so the time-averaged number of pulses is only 3 times larger. The second benefit of this SAR approach is that the waveform has a more complex signature which includes both a leading and trailing edge. Below we discuss measuring the arrival time of the waveform by fitting a parameterized model to the waveform. The more complex shape of the

SAR altimeter provides a more accurate constraint on the arrival time. This is helpful for achieving the 0.02 m range precision requirement discussed above.

Ocean Waves Of course the actual ocean surface has roughness due to ocean waves and swells. This ramp-like return power (Figure 5, top) will be convolved with the height distribution of the waves within the footprint to further smooth the return pulse and make the estimate of the arrival time of the leading edge of the pulse less certain. We can investigate the effects of wave height on both return pulse length and footprint diameter using a Gaussian model for the height distribution of ocean waves. This model provides and excellent match to observed wave height distributions as shown in Figure 6 from *Stewart* [*1985*].

$$G(h) = \frac{1}{\sqrt{2\pi\,\Delta h}}\ exp\left(-\frac{h^2}{2\,\Delta h^2}\right) \tag{9}$$

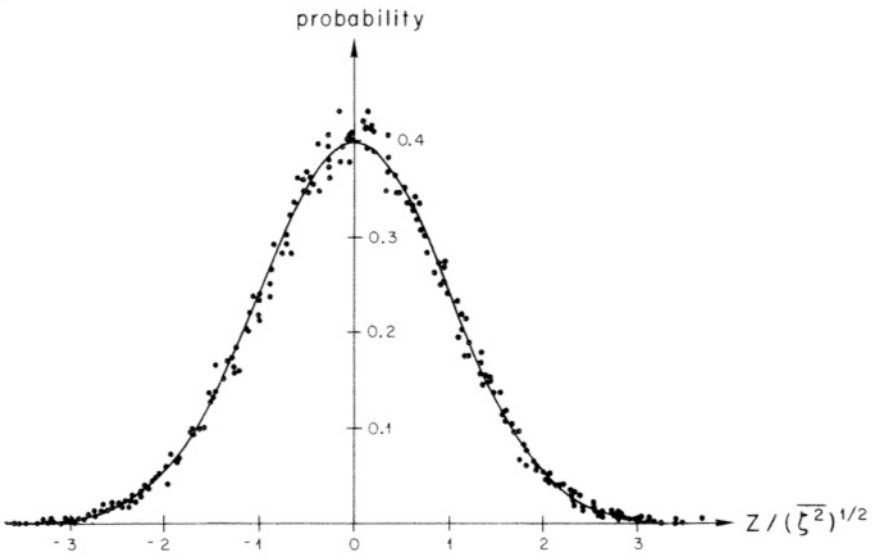

Figure 6. Probability distribution of sea surface elevation due to ocean waves normalized by the standard deviation of the wave height. This distribution is well fit by a Gaussian distribution. Wave height measured by observers on ships is equal to 4 times the standard deviation.

Approximately 1/3 of the waves will have height greater than Δh while 2/3 will have height less than Δh . An observer on a ship can accurately report the peak-to-trough amplitude of the highest

1/3 of the waves. Normally these waves will be $2\Delta h$ from the zero level; this is called the significant wave height and it is $h_{swh} = 4\Delta h$.

Now suppose we fly a narrow-bean altimeter (e.g., a laser) over this surface and observe the distribution of travel times. Assume that the beam-width of the laser is narrow enough to observe the topography of the wave field and we can map this into a distribution of two-way travel time.

$$h = \frac{c\,\tau}{2} \qquad G(\tau) = exp\left(\frac{-c^2\tau^2}{8\,\Delta h^2}\right) \tag{10}$$

Suppose we send a δ-function pulse. The probability distribution of the reflected pulse *O(t)* is the input pulse convolved with the Gaussian wave height model.

$$O(t) = \int_{-\infty}^{\infty} \delta(t)\; G(t-\tau)\; d\tau \;=\; G(t) \tag{11}$$

Now we can equate this to a wide-beam radar pulse as it reflects from the entire wave field within the footprint. There will be many waves within the > 1.7 km footprint so we can regard the radar return pulse as the average of all of the laser returns over the wave field. The radar return pulse width t_w is measured as the full width of the pulse where the power is 1/2.

$$\frac{1}{2} = exp\left(\frac{-2c^2\left(\frac{t_w}{2}\right)^2}{8\,\Delta h^2}\right) \quad \text{so} \quad t_w^2 = 16\,\frac{\Delta h^2}{c^2}\,ln\,2. \tag{12}$$

Since we were unable to form a very sharp radar pulse because the radar bandwidth is limited to 0.3 GHz, the total width of the return pulse will be established by convolving the outgoing pulse with the Gaussian wave model. If the outgoing pulse can also be modeled by a Gaussian function having a total pulse width of t_p, then the total width of the return pulse is given by

$t^2 = t_p^2 + \frac{h_{swh}^2}{c^2} \ln 2$. This provides and expression for the pulse width as a function of significant wave height (SWH). Similarly the diameter of the pulse as a function of significant wave height is $d = 2(cHt)^{1/2}$. Both functions are shown in Figure 7 SWH ranging from 1 to 10 m. It is clear that the quality of the altimeter measurement will decrease with increasing SWH. In practice we have found that Geosat, ERS, and Topex data are unreliable when SWH exceeds about 6 m.

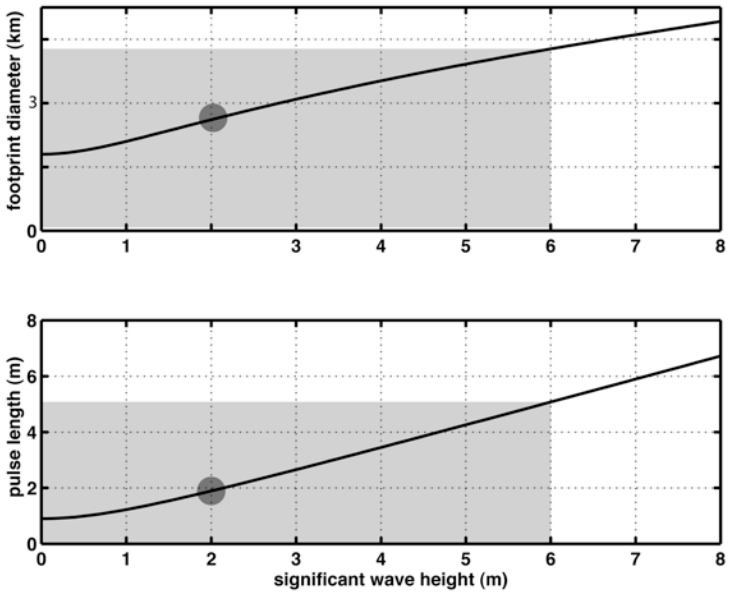

Figure 7. (lower) return pulse length in meters as a function of significant wave height. (upper) diameter of the radar pulse on the ocean surface as a function of significant wave height. A typical significant wave height of 2 m is marked by the large grey dot.

Significant Wave height is typically 2 meters so the radar footprint is typically 2.5 km and the pulse-width increases from 3 ns to 8 ns. Now we see that our original plan of having a very narrow pulse of 60 picoseconds to resolve 0.02 m height variations was doomed because the ocean surface is usually rough; a 3 ns pulse is all that could be resolved anyway. But how do we achieve the 0.02 m resolution needed for our applications when typically we can only resolve 1.2 m? The way to improve the accuracy by a factor of 10^2 is to average 10^4 measurements and hope the noise is completely random.

The speed of light provides an interesting limitation for space borne ranging systems. At a typical orbital altitude of 800 km it takes 5.2 milliseconds for the pulse to complete its round trip route.

One can have several pulses en-route but because we actually send a long chirp rather than a pulse, a pulse repetition frequency is limited to about 1000 pulses per second; during this time the altimeter moves about 7000 m along its track. Thus in each second there are 1000 pulses available for averaging; this will reduce the noise from 1.2 m to 0.04 m. Further averaging can be done for many of the oceanographic applications where the horizontal length scale of the feature is > 50 km. Of course one should be careful to remove all of the known signals using the full resolution data and then smooth the residual data along the profile to achieve the 0.02 m accuracy. (Please avoid the boxcar filter because it produces terrible sidelobes.)

Because of these limitations, single conventional altimeter profiles are unable to achieve the point-to-point accuracy of 0.02 m needed for high-resolution gravity field recovery. For this application one must rely on repeat or nearby profiles to gather the 10 samples needed to reduce the noise. Another promising approach to improved range precision is to use the SAR altimeter waveform as discussed above although this has not been tested to date (2011).

Modeling the Return Waveform There are a couple of other relevant engineering issues related to picking the travel time of the return pulse. First, after the return echo is passed through a matched filter to form the pulse, the pulse power is recorded at 64 times or *gates* in a window that is about 30m long. (Newer altimeters have 128 gates and a 60 m window.) An adaptive tracker is used to keep the power ramp in the center of the window. The ocean surface it typically smooth at length scales greater than the footprint so keeping the pulse in the window is not a problem. However, over land or ice, it is not usually possible to keep the pulse within the window because 30 m variations in topography over several kilometers of horizontal distance are quite common. Geosat and Topex altimeters lose lock over land and must re-acquire the echo soon after moving back over the ocean. The ERS-1/2 altimeters widen the gate spacing over land and ice so they can measure land topography as well as ocean topography. The analysis below is based on retracking of ERS-1 altimetry data but the same methods apply for other conventional mode altimeters. Retracking of the SAR altimeter waveforms is still a research area.

After recording the waveform of the return pulse, 50 echoes are averaged and an analytic function is fit to each waveform. A model for the expected power versus time is found by convolving the

flat surface response function shown in Figure 5 with a Gaussian wave height distribution. This results in an error function given by (*Brown*, 1977); (Amarouche *et al.*, 2004)

$$M(t,t_o,\sigma,A) = \frac{A}{2}\left[1 + erf(\eta)\right]\begin{cases} 1, & t<t_o \\ \exp\left[-(t-t_o)/\alpha\right], & t \geq t_o \end{cases} \quad (13)$$

where

$$\eta = \frac{(t - t_o)}{\sqrt{2}\sigma} \quad (14)$$

and where t is the time since the pulse was transmitted, t_o is the arrival time of the half power point of the returned energy, σ is the arrival rise time parameter, A is the amplitude of the returned waveform, and α is an exponential decay in the trailing edge due to the finite beam-width of the antenna. In addition to these four parameters, waveforms from some altimeters also show a background noise level.

The pointing accuracy of the ERS spacecraft was generally very good and the antenna mispointing was much less than the antenna beam-width, so we set this decay parameter α to a constant (137 nsec). The ERS-1 altimeter hardware truncated small power levels to zero (discussed below), and so we do not need a background noise level parameter. Therefore our retracking model for ERS-1 has only 3 free parameters, A, t_o, and σ. The automatic gain control loop in hardware maintained A at a relatively constant level, and the significantly variable parameters of chief concern in this paper are t_o and σ. In our model fitting, these are treated as non-dimensional parameters in dimensionless units of waveform sample gate widths; the physical time sampled by an ERS-1 waveform gate sample is 3.03 nsec of two-way travel time, corresponding to 0.4545 m of range to the sea surface. The rise width of the waveform, σ, is a convolution of the effective width of the point target response and the vertical distribution of ocean surface waves, usually parameterized in terms of a Gaussian standard deviation equal to 1/4 of the significant wave height, SWH as discussed above. An example model waveform for σ= 6.67 nsec (significant wave height of 3.6 m) is shown in Figure 8 (upper).

The objective of our analysis is to reduce the error in the estimated arrival time of the pulse, t_0. However before considering this problem one must understand the signal and noise characteristics of the return waveform. The ERS radar altimeter emits 1020 pulses per second and the returned power P_i is recorded in 64 gates spaced at 3.03 nsec. An onboard tracker is used to keep the pulse approximately centered in the travel-time window (gate 32) while 50 returned pulses are averaged. The averaged returned waveforms are available from the European Space Agency in the "WAP" data product, which also contains the onboard tracker's estimate of the expected range to the ocean surface used to align the waveforms.

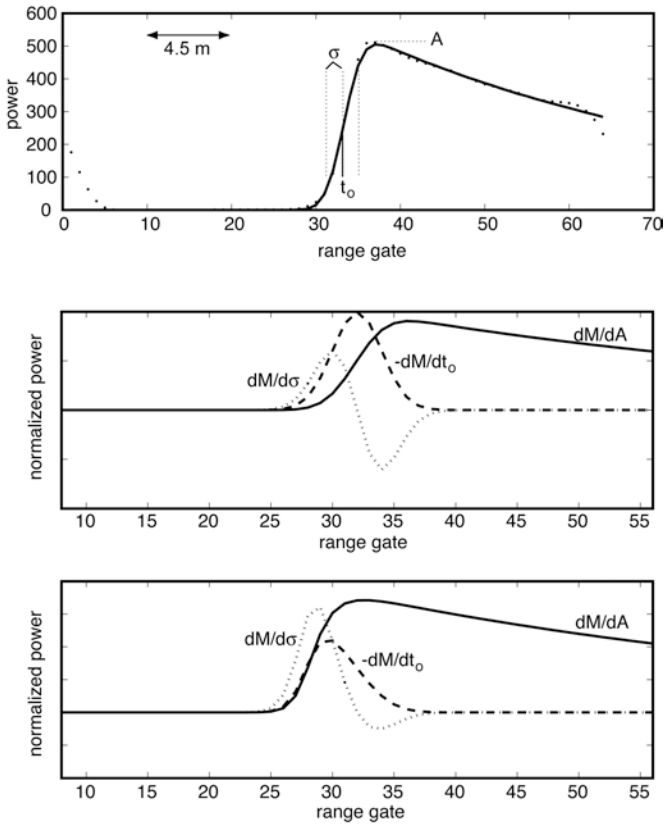

Figure 8. upper – average of 10,000 ERS-1 radar waveforms (dotted) and a simplified model (solid, equation 13) with three adjustable parameters: A-amplitude, t_o – arrival time, and σ – rise time. Time parameters are measured in dimensionless waveform gate widths equal to 3.03 nsec of two-way travel time or 454 mm of range to the sea surface.
middle - Partial derivatives of model (equation 17) with respect to A (solid), t_o (dashed) and σ (dotted) versus gate number. Note the functions dM/dt_0 and $dM/d\sigma$ are orthogonal. lower – Partial derivatives of the model waveform weighted by the expected uncertainty in the power (equation 17). Note the functions dM/dt_0 and $dM/d\sigma$ appear similar. This leads to a high correlation between arrival time and rise time during the least-squares estimation.

An individual radar pulse reflects from numerous random scatterers on the ocean surface so the return power versus time will be noisy - essentially following a Rayleigh scattering distribution. This high noise level is reduced in the 50 waveform average. Assuming the speckle is incoherent from pulse-to-pulse, this incoherent average will reduce the speckle noise by a factor of $\sqrt{50}$. The averaging of 50 pulses combined with a computer bug which truncated the pre-arrival data leads to the following functional form for the uncertainty in the power W_i as a function of the recorded power P_i

$$W_i = \frac{\left(P_i + P_o\right)}{\sqrt{K}}$$

K is the number of statistically independent waveforms used in the average and P_o is the offset due to the truncation. Our Monte-Carlo simulation of the truncation process and our experiments in optimizing the retracking of real ERS waveforms led us to use K = 44 and P_o = 50, which is essentially the same weighting used by *Maus et al.,* (1998). While the results are largely insensitive to the exact numerical values for N and P_o, the functional form of this uncertainty leads to a high correlation between the arrival time and the rise time when they are estimated using a weighted least squares approach. Overcoming this correlation is the essence of a study by *Sandwell and Smith* [2005].

A standard least-squares approach is used to estimate the 3 parameters (t_o, σ, and A). Because the problem is non-linear in arrival time and SWH, we use an iterative gradient method. The chi-squared measure of misfit is

$$\chi^2 = \sum_{i-1}^{N} \left[\frac{P_i - M_i(t_o, \sigma, A)}{W_i} \right]^2 \qquad (15)$$

where N is the number of gates used for the fit and M_i is the model evaluated at the time of the i^{th} gate. One starts the iteration by subtracting a starting model based on parameters t_o^o, σ^o, and A^o.

The updated model parameters t_o^1, σ^1, and A^1 are found by solving the following linear system of equations

$$\begin{bmatrix} P_1' \\ P_2' \\ \vdots \\ \vdots \\ P_N' \end{bmatrix} = \begin{bmatrix} \frac{\partial M_1}{\partial t_o} & \frac{\partial M_1}{\partial \sigma} & \frac{\partial M_1}{\partial A} \\ \vdots & \vdots & \vdots \\ \vdots & \vdots & \vdots \\ \frac{\partial M_N}{\partial t_o} & \frac{\partial M_N}{\partial \sigma} & \frac{\partial M_N}{\partial A} \end{bmatrix} \begin{bmatrix} t_o^1 - t_o^o \\ \sigma^1 - \sigma^o \\ \vdots \\ A^1 - A^o \end{bmatrix} \tag{16}$$

where P_i' is the waveform power minus the model from the previous iteration. The derivatives of the model with respect to the parameters are

$$\frac{\partial M}{\partial t_o} = \frac{-A}{\sigma\sqrt{2\pi}} e^{-\eta^2}$$

$$\frac{\partial M}{\partial \sigma} = \frac{-A}{\sigma\sqrt{\pi}} \eta e^{-\eta^2} \tag{17}$$

$$\frac{\partial M}{\partial A} = \frac{M}{A}$$

We have not included the complications of the exponential decay in the partial derivatives of equation 1 because this effect is largely removed with the starting model, and because residual misfits in the plateau of the waveform are chiefly random and do not significantly drive the fit of the 3 important parameters. These partial derivatives are shown in Figure 8 for the case of an unweighted and weighted least-squares adjustment. A standard Newton iteration algorithm is used to determine the three model parameters (t_o, σ, A) that minimize the rms misfit. Of course the arrival time t_o provides the range estimate. The rise time σ provides and estimate of SWH. The amplitude (called sigma-naught -σ_o) provides an estimate of surface roughness at the 20-30 mm length scale. This latter measurement can be related to surface wind speed since wind will roughen the ocean surface. Precise calibration is performed for each of the three measurements.

Absolute range calibration is performed in the open ocean using an oil platform having a GPS receiver and accurate tide gauge. Both SWH and wind speed are calibrated using open-ocean shipboard measurements

Corrections

Sea State Bias - This is perhaps the most insidious problem for monitoring global sea level changes over long periods of time. While the topography of open ocean waves is quite symmetric, the crests of the waves preferentially scatter the radar waves outward away from nadir while the troughs of the waves focus the energy back toward the radar. This skews the ramp of the radar return toward later times. This effect is sometines called the E/M bias and it is typically 5% of the SWH. This correction is highly uncertain and poorly understood. Wave height varies seasonally so this correction can easily introduce a 0.05 - 0.10 m bias in estimates of large scale dynamic topography.

Ionospheric Delay - We have already discussed how the electron plasma in the ionosphere slows the group velocity of the radar pulse. The homework problem in Rees, Ch3, #3, is to derive an expression relating the total electron content (TEC) in the nadir direction to the travel time difference between pulses at 2 and 5 GHz. The attached plot shows how electron density varies with altitude at different times of the day. The smallest ionospheric correction occurs at 6 AM while the largest correction is at 12 noon. The dual frequency correction scheme is quite accurate over large length scales (> 50 km) but at shorter wavelengths the correction can actually add noise to the range measurement; we don't apply this correction when computing gravity anomalies from satellite altimetry. Also note that the TEC has an eleven year cycle; the next peak is in 2002.

Dry Atmosphere - The index of refraction of the dry atmosphere is simply related to the surface temperature and pressure. The water vapor causes and additional delay. The total correction is:

$\Delta h = 2.27 \times 10^{-5} P_s + 1.723 W/T_a$ where

Ta - air temperature (˚K)

W - zenith water vapor (kg m^{-2})

Ps - surface pressure (Pa)

Typical values of dry tropospheric delay are 2.3 m while the wet delay can vary from 0.06 - 0.30 m

Orbit Error - Until 1992, radial orbit error was the major limitation of satellite altimetry. Back in 1978 when Seasat was in orbit, the best radial orbit accuracy was about 1 m rms. Nowadays GPS tracking provides radial orbit error of 0.02m rms. Even altimeters without GPS tracking have radial orbital accuracy of about 0.07 m.

Dual Frequency Altimeter A dual frequency altimeter is used to measure the ionospheric delay and then apply the correction to the range measurement. Here is an example from problem 3 of chapter 4 in Rees:

A dual frequency altimeter emits short pulses at 2 GHz and 5 GHz. Beacuse the ionosphere is dispersive, the reflected pulses are separated in time by 15 ns. Calculate the total electron content of the ionosphere.

The total electron content N_T has units of electrons per area and thus it is the integral of the electron density N_e from the ocean surface to the height of the spacecraft H.

$$N_T = \int_0^H N_e(z)\, dz \tag{18}$$

The round trip travel time of the radar pulse T is

$$T = 2\int_0^H \frac{1}{v_g(z)} dz \tag{19}$$

where v_g is the velocity of the pulse. When the radar angular frequency ω is much greater than the plasma frequency, the index of refraction is approximately

$$n'(z) \cong 1 - \frac{N_e(z)\, e^2}{2\, \varepsilon_o m\, \omega^2} \tag{20}$$

N_e - electron density
e - electron charge
m - electron mass
ε_o - permittivity of free space
ω - radar angular frequency (radians/second)

The phase velocity of the radar wave is $v_p = \frac{c}{n'}$ and it exceeds the speed of light. However, the pulse travels at the group velocity $v_g = \frac{d\omega}{dk}$ which is less than the speed of light. With a little algebra one can arrive at the group velocity.

$$v_g = c\left[1+\frac{N_e e^2}{2\varepsilon_o m\omega^2}\right]^{-1} \tag{21}$$

The travel time difference Δt can be written as

$$\Delta t = T_2 - T_5 = \frac{2}{c}\int_o^H \left\{\left[1+\frac{N_e e^2}{2\varepsilon_o m\omega_2^2}\right]-\left[1+\frac{N_e e^2}{2\varepsilon_o m\omega_5^2}\right]\right\} dz \tag{22}$$

or

$$\Delta t = \frac{e^2}{mc\varepsilon_o}\left[\frac{1}{\omega_2^2} - \frac{1}{\omega_5^2}\right]\int_0^H N_e(z)\, dz \tag{23}$$

Note that the integral on the right side is the total electron content so solving for the TEC one finds

$$N_T = \Delta t\, \frac{mc\varepsilon_o}{e^2}\left[\frac{1}{\omega_2^2} - \frac{1}{\omega_5^2}\right]^{-1} \tag{24}$$

Plugging in the numbers one finds that for a 15 ns delay, the TEC is 2.52×10^{17} electrons m^{-2}. It is interesting to calculate the total delay of a microwave signal as a function of frequency for this TEC.

frequency (GHz)	wavelength (mm)	band	2-way delay (m)
1	300	P	20
2	150	L	5
5	60	C	0.8
10	30	X	0.2
13	23	Ku	0.1

It is clear that ionospheric delay is a major source of error for all active microwave ranging systems, especially those operating at longer wavelength.

References

Amarouche, L., Thibaut, P., Zanife, O.Z., Dumont, J.-P., Vincent, P. & Steu- nou, N., 2004. Improving the Jason-1 ground retracking to better account for attitude effects, Marine Geodesy, 27, 171–197.

Brown, G.S., 1977. The average impulse response of a rough surface and its application, IEEE Transactions on Antenna and Propagation, AP-25(1), 67–74.

Maus, S., Green, C.M. & Fairhead, J.D., 1998. Improved ocean-geoid res- olution from retracked ERS-1 satellite altimeter waveforms, Geophys. J. Int., 134(N1), 243–253.

Geosat Issue I, *J. Geophys. Res.*, v. 95, C3, p.2833-3448, 1990.

Geosat Issue II, *J. Geophys. Res.*, v. 95, C10, p.17865-18367, 1990.

Raney, R. K., The Delay/Doppler Radar Altimeter, IEEE TRans. Geoscience and Remote Sensing, V. 36, p. 1578-1588, 1998.

Seasat Special Issue I: Geophysical Evaluation, J. Geophys. Res., v. 87, C5, p. 3173-3431, 1982.

Seasat Special Issue II: Scientific Results, J. Geophys. Res., v. 88, C3, p. 1529-1937, 1983.

Sandwell, D. T., and W.H.F. Smith, Retracking ERS-1 Altimeter Waveforms for Optimal Gravity Field Recovery, Geophys. J. Int., 163, 79-89, 2005.

Special Topex/Poseidon Issue of JGR, 1996

Stewart, R. H., Methods of Satellite Oceanography, University of California Press, Berkeley, CA, 1985.

The Navy GEOSAT Mission, Johns Hopkins APL Technical Digest, v.8, no. 2, 169-267, April-June, 1987.

Walsh, E. J., E. A. Uliana and B. S. Yaplee, Ocean wave heights measured by a high resolution pulse-limited radar altimeter, Boundary Layer Meterology, V. 13, p. 263-276, 1978.